Pergamon

Int. J. Heat Mass Transfer. Vol. 39, No. 3, pp. 547–561, 1996

0017-9310/96 $9.50+0.00

0017-9310(95)00138-7

An experimental investigation on natural and forced convection in liquid metals

STAVROS A. ARGYROPOULOS

Department of Metallurgy and Materials Science, University Of Toronto, Toronto, Ontario, Canada M5S 1A4

and

ANTHONY C. MIKROVAS

Cominco Ltd, Trail, British Columbia, P.O. Box 2000, Canada V1R 4S4

(*Received* 7 *September* 1994 *and in final form* 21 *March* 1995)

Abstract—This paper presents a method for deducing dimensionless heat transfer correlations in liquid metals for natural and forced convection conditions. This method was applied to liquid metals with different Prandtl numbers, namely, aluminum and steel. Solid spheres of aluminum and steel, initially at room temperature, were immersed into liquids of aluminum and steel, respectively. In the first set of tests the spheres were immersed under natural convection conditions, and in the second, under forced convection conditions. The melting time of the spheres was carefully monitored and it was related to the average heat flux from the metal bath to the immersed sphere.

INTRODUCTION

There is a plethora of published research in the area of natural convective heat transfer to and from various objects, which are immersed in fluids. Yet, there is a scarcity of work involving liquid metals. Theoretical and experimental approaches have been applied to quantify the convective heat transfer in fluids. In one theoretical approach, Raithby and Hollands [1] proposed that the local heat transfer in laminar and turbulent flow is controlled locally by a balance of viscous and buoyancy forces near the wall. With this hypothesis, an equation for the local conduction thickness was derived. For the case of spheres the following correlation was suggested:

$$\overline{Nu_D} = 2+0.56\langle Pr/(0.846+Pr)\rangle^{0.25} * Ra_D^{0.25}. \quad (1)$$

However, the above equation was tested in fluids with a Prandtl number of only 0.72.

Using a different theoretical approach Churchill [2] recommended the following correlation for laminar free convection from spheres:

$$\overline{Nu_D} = 2+\frac{0.589 * Ra_D^{0.25}}{\langle 1+(0.43/Pr)^{9/16}\rangle^{4/9}}. \quad (2)$$

The same author [2] claims that equation (2) provides a good approximation for $Gr < 10^9$ and for all Prandtl numbers. The theoretical ramifications of the usage of liquid metals as coolants in nuclear reactors are reviewed by Stein [3]. A comprehensive review of relevant experimental work in liquid metals is given in refs. [4] and [5]. Most of this work has been done in low melting-point metals. Spheres as well as cylinders were used as immersed objects in liquid metals. Numerous research studies on convective heat transfer to or from spheres in fluids were carried out with fluids whose Prandtl number was not less than 0.7 [6–10]. Mass transfer work from spheres to various fluids, under natural convection conditions, has also been reported [11–15]. The fluids involved in these tests [6–15] have higher Prandtl numbers from those of liquid metals, which render their applicability to liquid metals inappropriate.

In an effort to quantify the forced convective heat transfer to or from spheres immersed in fluids, both theoretical and experimental approaches have been undertaken. In one theoretical approach, the boundary-layer theory was used [16], but as the author acknowledged, the theoretical solution converges only as long as the Prandtl number is greater than 2. Hsu [17] and Sideman [18] have derived theoretical Nusselt numbers for the case of heat transfer to liquid metals flowing past a single sphere, their analyses were based on the assumption associated with inviscid potential flow. Equations (3) and (4) represent results by Hsu [17] and Sideman [18], respectively:

$$\overline{Nu_D} = 0.921 * Re^{0.5} * Pr^{0.5} \quad (3)$$

and

$$\overline{Nu_D} = 1.13 * Re^{0.5} * Pr^{0.5}. \quad (4)$$

It is noteworthy, that although both Hsu and Sideman address the identical problem and both use a theoretical approach, their results differ by 22%. A few

NOMENCLATURE

A	average surface area of the sphere during its immersion in metal bath [m]
C_p	heat capacity [J kg^{-1} K^{-1}]
D	sphere diameter [m]
Δt	sphere melting time [s]
ΔH	heat required to raise the unit mass of the immersed sphere from room temperature up to its melting point plus the latent heat of fusion [kJ kg^{-1}]
g	gravitational acceleration [9.807 m s^{-2}]
h_D	average heat transfer coefficient for a sphere [W m^{-2} K^{-1}]
k	thermal conductivity [W/m K]
m	immersed mass of sphere [kg]
q''_D	average heat flux from liquid metal to sphere [kW m^{-2}]
V	tangential velocity [m s^{-1}]
SPH	metal bath superheat, $T_{mp}-T_{melt}$ [K]
T_f	film temperature, $(T_{mp}+T_{melt})/2$ [K]
T_{mp}	melting point temperature [K]
T_{melt}	melt temperature [K].

Greek symbols

β	Coefficient of thermal expansion [K^{-1}]
ρ	Density [kg m^{-3}]
μ	Viscosity [kg s^{-1} m^{-1}].

Dimensionless groups

$\overline{Nu_D}$	average Nusselt number for a sphere, $h_D D/k$
Re	Reynolds number, $DV\rho/\mu$
Pr	Prandtl number, $C_p\mu/k$
Gr_D	Grashof number, $\beta g D^3\rho^2$ SPH$/\mu^2$
Ra_D	Rayleigh number, $Pr*Gr_D$.

experimental investigations have also been undertaken in various attempts to quantify the forced convective heat transfer. The work by Kreith *et al.* [19] underscores the importance of a given fluid's Prandtl number for convective heat transfer. Kreith *et al.* [19] measured significant differences in forced convective heat transfer in spheres which were cooled in oil ($Pr = 217$), water ($Pr = 4.52$), air ($Pr = 0.72$) and mercury ($Pr = 0.024$). They suggested the following correlations:

$$\overline{Nu_D} = 0.43*Re^{0.5}*Pr^{0.4}$$

For $[Gr < 0.1Re^2, Re < 5\times10^5, 0.7 < Pr < 217]$ (5)

and

$$\overline{Nu_D} = 0.066*Re^{0.67}*Pr^{0.4}$$

For $[Gr < 0.1Re^2, 5\times10^5 < Re < 7\times10^6, 0.7 < Pr < 7]$. (6)

In the same work, Kreith *et al.* [19] suggested a dimensionless correlation to describe the sphere cooling in liquid mercury, which is substantially different from the fluids having higher Prandtl numbers:

$$\overline{Nu_D} = 0.178*Re^{0.375}$$

for $[7\times10^4 < Re < 10^6, Pr = 0.024]$. (7)

In their experimental findings, Kreith *et al.* suggested that there is no difference between heating and cooling of spheres in water [19]. Witte presents another dimensionless correlation, which is based on experiments of forced convection heat transfer from a sphere to liquid sodium [20]. The following dimensionless equation was proposed:

$$\overline{Nu_D} = 2+0.386*(Re*Pr)^{0.5}$$

for $[3.56\times10^4 < Re < 1.525\times10^5, Pr \approx 0.004]$. (8)

In the same work a very interesting comparison is presented. The results in liquid sodium are presented against results derived from a similar correlation introduced by Vliet and Leppert [21], which was derived from experimental work with water. The results in liquid sodium [20] were appreciably lower than those results derived from the suggested correlation of Vliet and Leppert [21]. Similarly, correlations reported by Kreith *et al.* [19] for liquid mercury were much lower than those obtained in oil, water and air. Consequently various comparisons of different fluids under forced convection conditions suggest that all liquid metals do not behave similarly.

The present study has two main objectives: (1) to develop a method for studying natural and forced convection in the harsh liquid metal environment and (2) to develop semi-empirical correlations for various types of convective heat transfer in liquid metals. This objective was accomplished by applying this method developed to liquid metals with different Prandtl numbers.

EXPERIMENTAL METHODOLOGY

Two different liquid metals were used in this experimental work, aluminum and steel. There are many similarities in the experimental procedures used with both metals. First, the experimental procedure for

liquid aluminum will be presented. Then, only the points for which the experimental procedure of liquid steel differs from that of liquid aluminum will be pointed out. In addition the methodology for the natural convection condition will be presented in detail, and for the forced convection, only points of departure will be mentioned.

Part I, *Natural convection experiments*

Aluminum was melted down in an induction furnace. Figure 1(A) shows a schematic cross section of the crucible along with its dimensions. Solid spheres of aluminum were used. The sphere was attached to a stainless steel holder. The solid sphere and the stainless steel holder form the sphere assembly. Figure 2 displays the various parts of the sphere assembly as well as the complete sphere assembly. The drilled portion of the cylindrical cavity of sphere represents 7% of its volume. As seen, a zirconia tube provided a link between the holder and the lower stainless steel part. The low thermal conductivity of the zirconia tube (2.5 $W m^{-1} K^{-1}$) as well as its rather reasonable resistance to thermal shock, were the prime reasons for the selection of this material. A very important feature of the sphere assembly was an internal thermocouple. The tip of this thermocouple was intentionally positioned within the cylindrical cavity without touching the walls of the cavity. This is shown in the schematic diagram of the complete sphere assembly shown in Fig. 2. This arrangement allowed a very accurate detection of the sphere melting time. The exact time of the sphere immersion in the bath was recorded with an external thermocouple. The sphere was always immersed at point P. The coordinates of this point are depicted in Fig. 1(A). The liquid aluminum temperature was measured with two K-type thermocouples which were positioned at different locations inside the alumina crucible. Measuring the bath temperature at two different locations allows for the detection of any non-isothermal conditions in the aluminum bath. The experiment proceeded only when isothermal conditions existed.

Armco Iron was melted down in a similar crucible to the one used for aluminum. The nominal composition of Armco Iron was 0.02–0.03 wt% C, 0.05 wt% Mn, 0.007 wt% P, 0.018–0.01 wt% S, 0.001 wt% Si and balance iron. Upon melting the Armco Iron was fully deoxidized. The steel bath preparation is outlined in more detail in ref. [22]. The spheres were made of steel of approximately the same chemical composition as the steel bath. The sphere assembly for the experiments in liquid steel is similar to the aluminum sphere assembly. In this case, however, there is a difference in the selection of materials. The material that was selected for the sphere holder for these studies was boron nitride (HP grade supplied by Carborundum Corporation) instead of stainless steel. A schematic diagram of the steel sphere assembly is given in Fig. 3. It consists of a steel sphere with a diameter 2.5 cm (with a cavity identical to that of the aluminum sphere shown in Fig. 2), which is screwed to the threaded end of the boron nitride holder. The length of the boron nitride cylinder is 14 cm, while its diameter is 1.9 cm. A bore is drilled along the centerline of this part allowing for an R-type thermocouple to be inserted in the sphere cavity. A steel holder is screwed to the upper end of the boron nitride holder allowing for the other end of the steel holder to be connected to the immersion apparatus. The liquid steel temperature was measured with a DT-250 thermoprobe made by Electro-Nite Corporation. This thermoprobe is specially designed for liquid steel, and provides an intermittent type temperature measurement. It has a long assembly and at the far end of this assembly a DipTip R-type thermocouple is inserted. It has been successfully applied in another research work which involved liquid steel [23]. In this work [23], it was found that the liquid steel temperatures measured with this DT-250 digital thermoprobe, were within 10°C of those measurements taken by a thermocouple assembly, which was continuously immersed in the liquid steel. The steel bath temperature was checked immediately before and after each experiment. The maximum temperature drop recorded was 10°C. In the presentation of the liquid steel results in the next section, the steel bath temperature reported is the average value of the temperature measurements performed as described previously.

In both liquid metals, the execution of a typical experiment included:

(1) Bringing the metal bath to the desired temperature.

(2) Turning off the induction furnace for a sufficient time, so that there is no flow in the bath due to the electromagnetic body forces.

(3) Immersing the sphere assembly to the desired depth in the liquid metal.

(4) Collecting the data from sensors with a data acquisition system. Figure 4 depicts schematically the data collection system used.

Part II, *Forced convection experiments*

The same liquid metals and crucibles used for Part I were used in Part II. The liquid metal preparation as well as the sphere assembly were identical with Part I. For this set of experiments the sphere assembly was rotating inside the liquid metal with a specific tangential velocity, in contrast to the natural convection condition where it was stationary. For both sets of conditions, the immersion point of the sphere was the same. Figure 1B depicts in a schematic way the rotating sphere in the metal bath. The experimental setup for stirring spheres in liquid metals is shown in Fig. 5. For this set of experiments, the execution of a typical test includes the four steps, which were outlined in the experimental plan of Part I. The precise measurement of the sphere's tangential

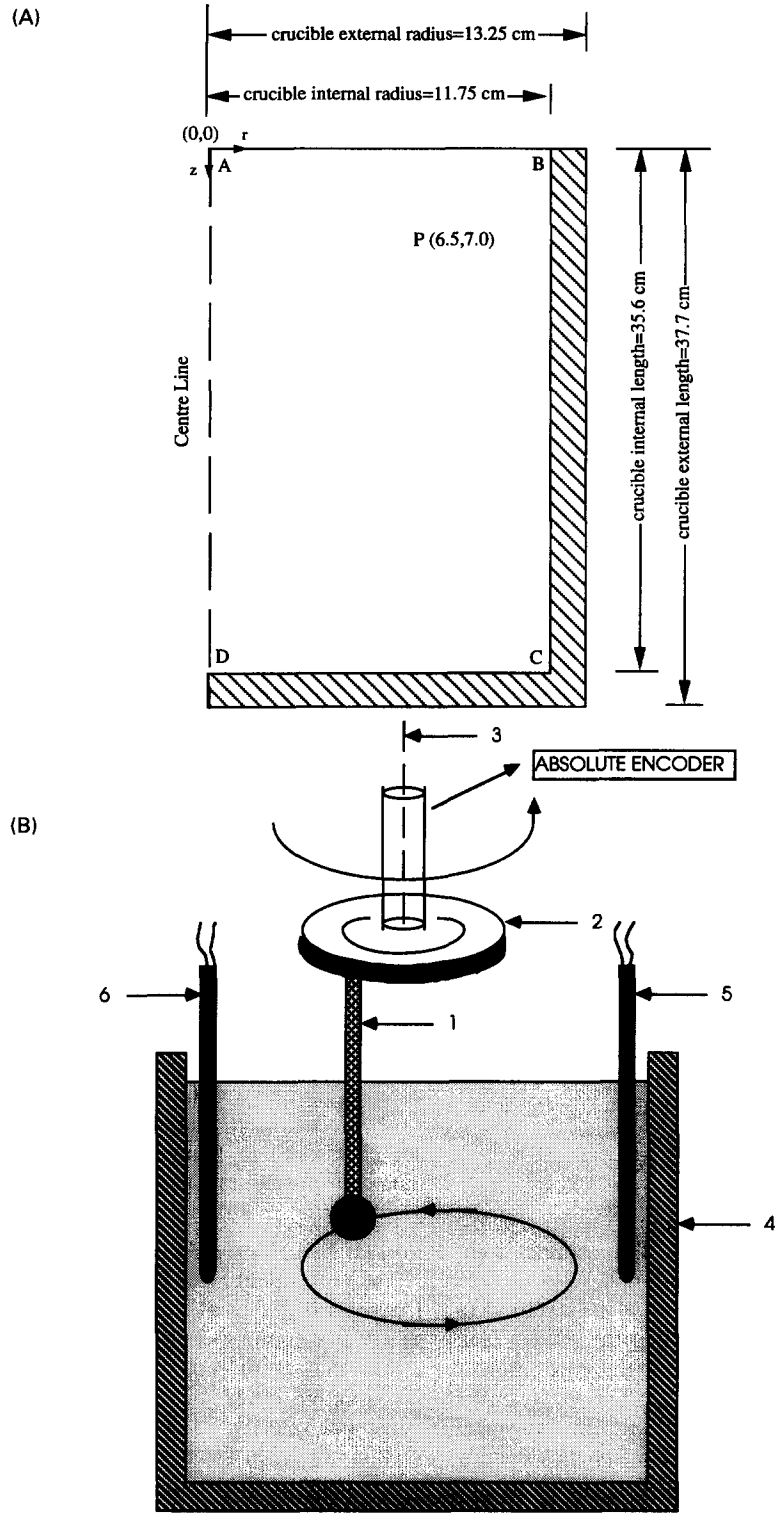

Fig. 1. (A) Cross-section of crucible used along with its dimensions. (B) Schematic cross-section of the container of liquid metal which shows the rotating sphere. 1, Sphere holder; 2, disc; 3, hollow shaft at the end of which the slip ring assembly was connected; 4, crucible; 5 and 6, bath thermocouples.

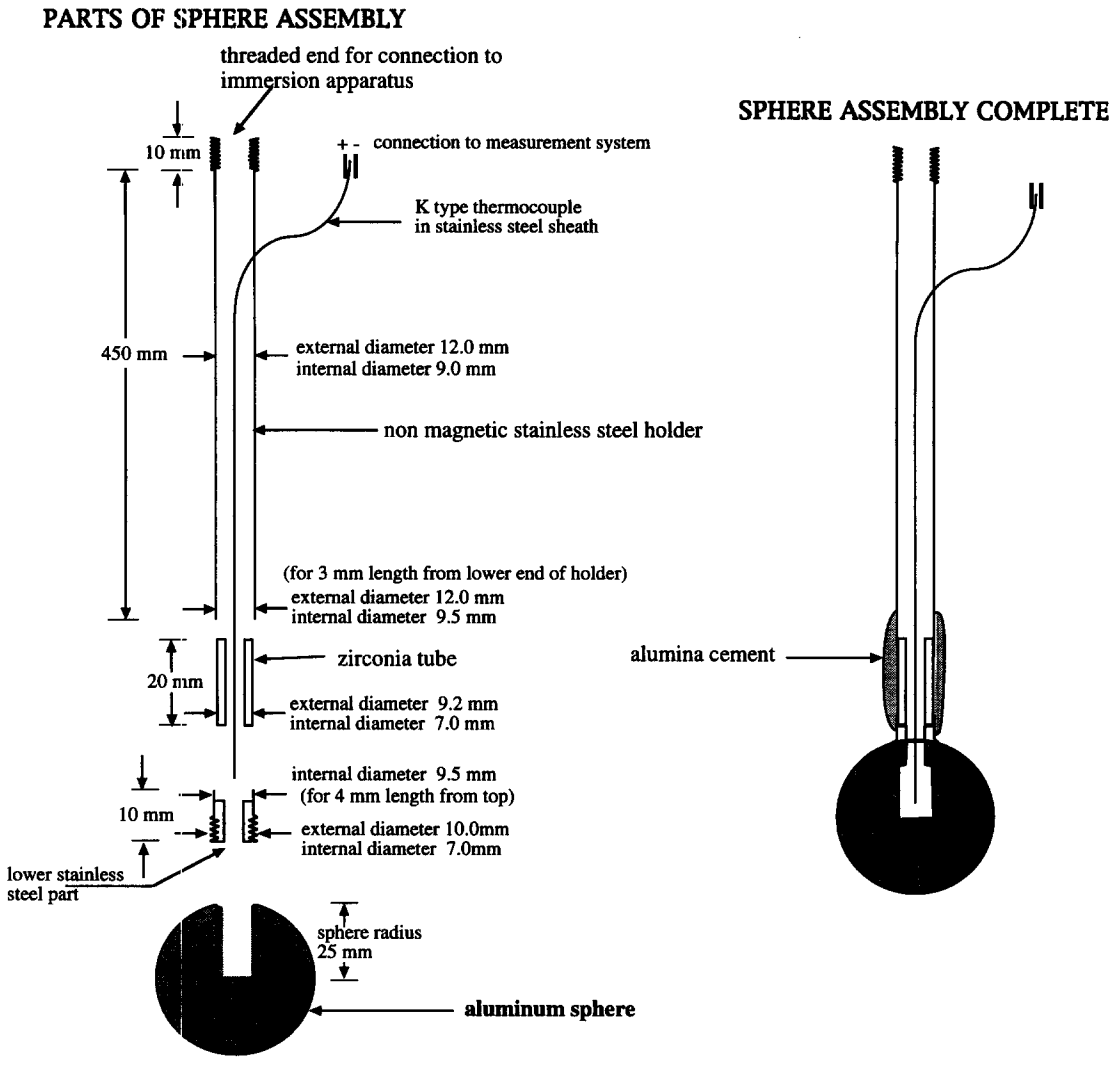

Fig. 2. Schematic diagram of various parts of assembly and a complete sphere assembly for aluminum experiments.

velocity was carried out with an absolute encoder, model AR-23 [24], which was interfaced with the data acquisition system shown in Fig. 4.

RESULTS FOR PART I. NATURAL CONVECTION

Aluminum

Figure 6A presents a typical experimental result for liquid aluminum. Two representative bath temperature readings are shown by curves (1) and (2), which clearly demonstrate that the difference between them is in the range of the accuracy of the K-type thermocouples that were used. Curve (4) is the temperature profile of an external thermocouple. It is initially suspended in air, segment AB, and it hits the surface of the hot water, segment BC, simultaneously with the immersion of the sphere into the liquid metal. Finally it stays at a constant temperature, segment CD, during the period the sphere is inside the aluminum melt. Curve (3) is the temperature profile recorded by the sphere thermocouple positioned as shown in Fig. 2. Segment EF records the temperature at the thermocouple tip location in the sphere cavity before the probe is immersed in the bath. Point F is taken as the immersion point [projection of point B on curve (3)]. Segment FG corresponds to the lag of the sphere thermocouple to record the immersion of the sphere in a high temperature environment. This occurs because the thermocouple tip is intentionally stationed in the air, inside the drilled cavity of the sphere. Segment FGH characterizes the heating period of the sphere. At point H the slope of the curve changes dramatically. The extremely large difference between the thermal conductivity of the air and of the liquid aluminum is responsible for this dramatic change in the slope. The slope change indicates that the liquid metal penetrates the sphere cavity. In an extremely short time interval the thermocouple records the melting temperature of aluminum [660.2°C, curve (5)] at point I, the intersection point of curves (5) and (3).

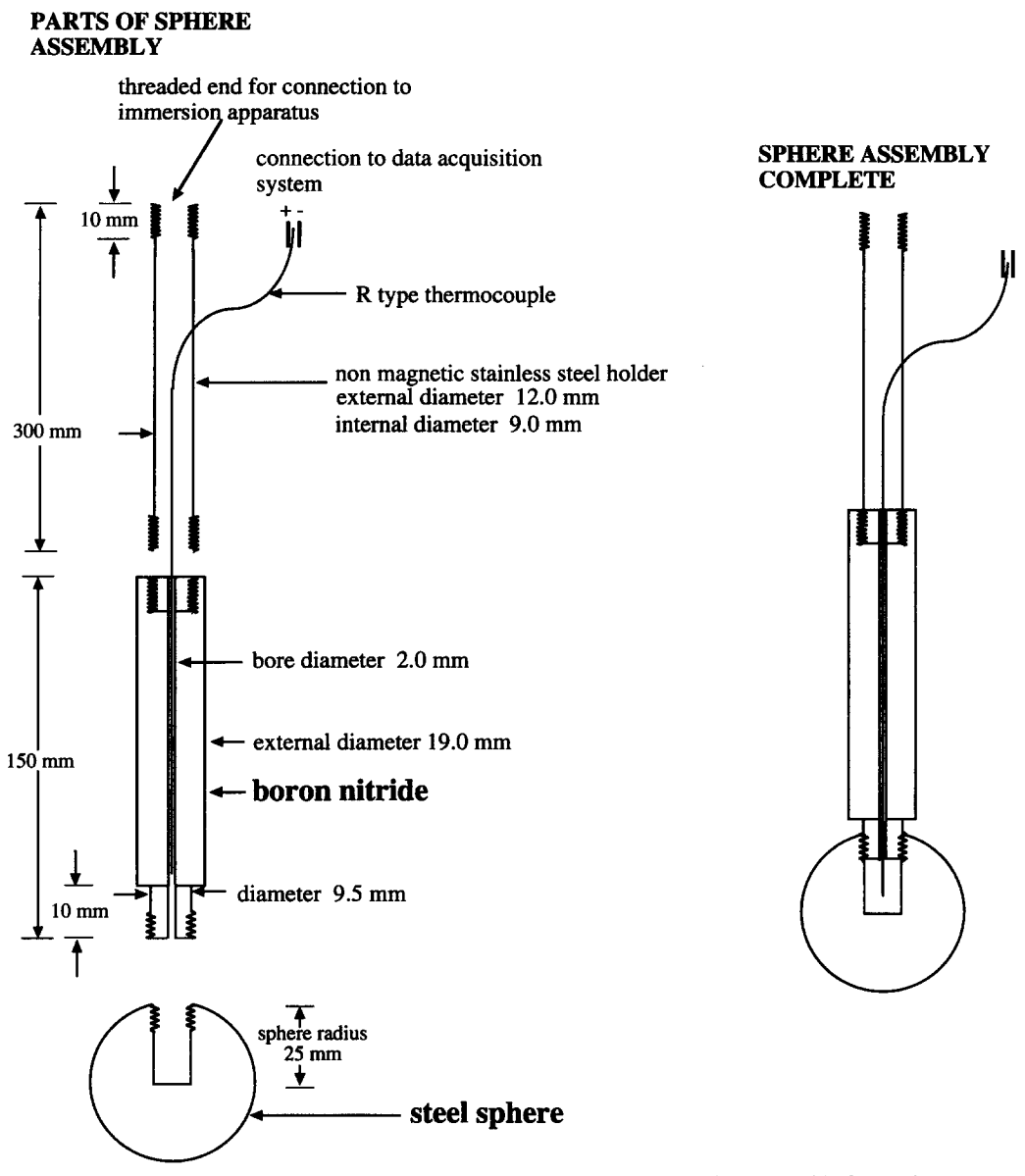

Fig. 3. Schematic diagram of various parts of assembly and a complete sphere assembly for steel experiments.

Segment IJ corresponds to the heating of the thermocouple tip above the aluminum melting point. It should be mentioned that the sphere thermocouple should finally record the local bath temperature, denoted by segment JK. The actual local bath temperature is presented by curve (6), and is recorded by an independent K type thermocouple at the end of the experiment. The reason for the difference (20–30°C) between the reading of the sphere thermocouple and the one shown in curve (6), was attributed to the slip ring assembly–temperature compensation system, through which the sphere thermocouple signal was transmitted to the data acquisition system. From the above analysis it can be seen that the time it takes for the sphere to melt can be determined by the projection of points B and I on the time axis, that is, segment RS. It should also be mentioned that there is a need for recording the temperature at the surface of the sphere before immersion. Such measurements were taken prior to each experiment using K-type thermo-

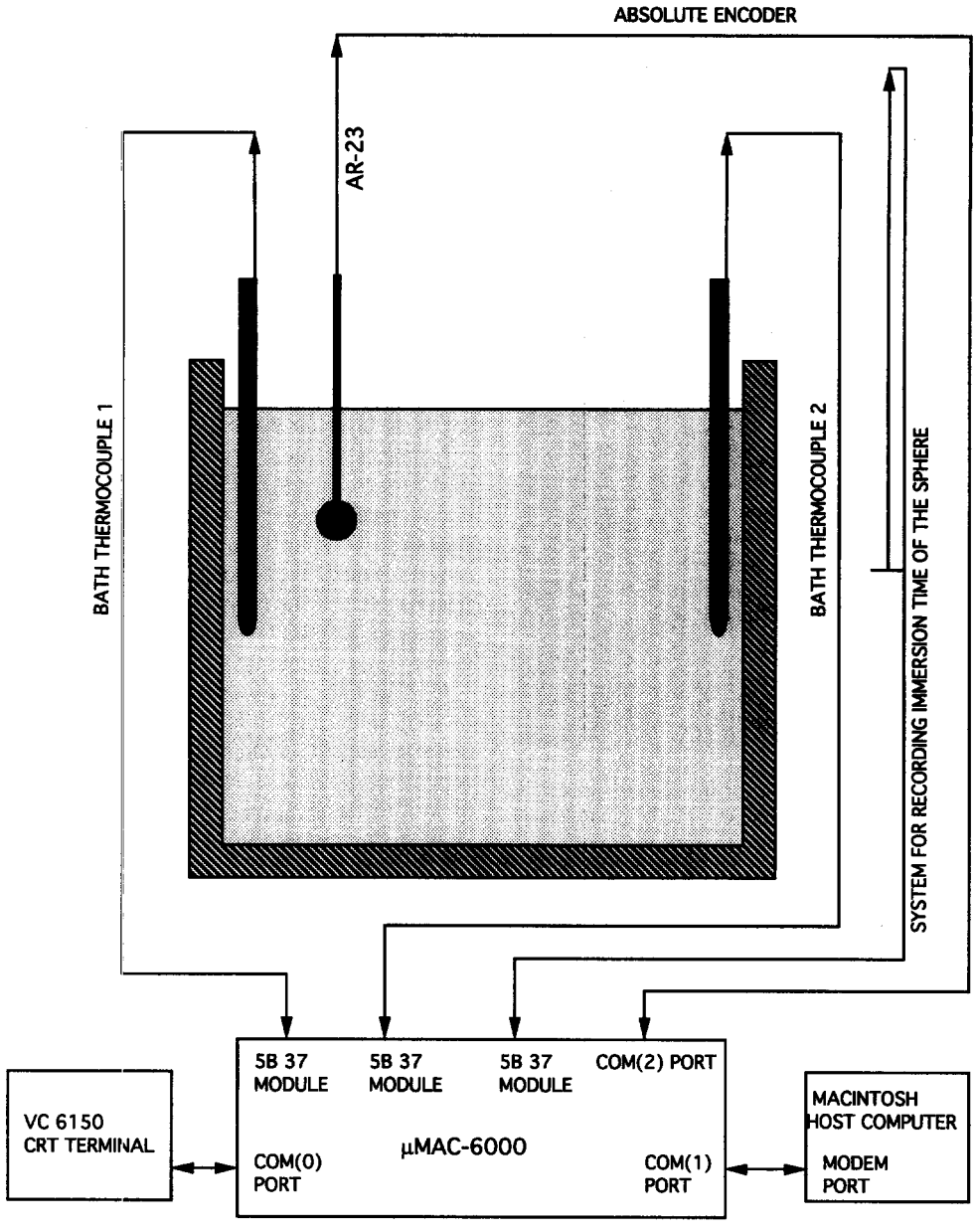

Fig. 4. Schematic diagram showing various sensors as well as the computer system used to capture the signals generated by these sensors.

couples. The average surface temperature of the sphere was in the range of 40–50°C for the bulk of the experimental work reported in this study.

Steel

Figure 6(B) presents a typical experimental result for liquid steel. The liquidus temperature was estimated to be 1520°C [25]. The calculation of the melting time is similar to the one presented in Fig. 6(A). In this case, the difference is that the liquidus temperature is 1520°C, while at point K, the thermocouple tip is destroyed (the symbols used in Figs 6(A) and (B) are identical).

Figures 6(A) and (B) illustrate how the melting time (Δt) was deduced from each experimental result. The amount of heat which is transferred from the metal bath to the sphere is equal to the heat which is required to melt the sphere, as expressed in a simple heat balance:

$$q''_D * A * \Delta t = m * \Delta H. \quad (9)$$

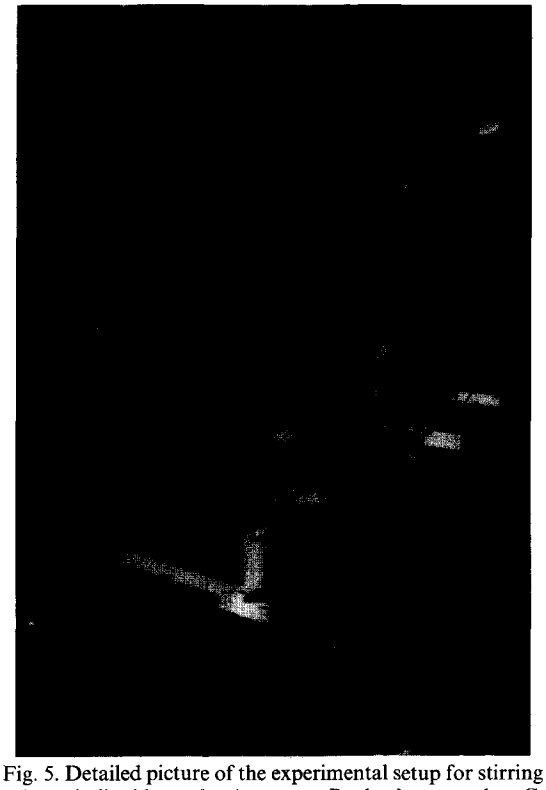

Fig. 5. Detailed picture of the experimental setup for stirring spheres in liquid metals: A, motor; B, absolute encoder; C, chain; D, gears; E, hollow shaft and F, aluminum block.

ΔH values for the metals used are given in Appendix A. In the first stage, the data were reduced from temperature–time measurements to Δt. In the second stage, the heat transfer rate for each experimental run was estimated using the findings of the first stage. The various thermal and physical properties used in the later stage are outlined in Appendix A. In calculating the estimate for the second stage, the drilled portion of the cylindrical cavity of the sphere as well as the surface area of the associated spherical cap were taken into account. For the correct estimation of the average heat fluxes the proper calculation of the average surface area of the sphere (i.e. A) is of great importance. When the sphere is immersed in a liquid metal, a solidified layer (shell) from the bath is formed which surrounds the sphere, and therefore the surface area of the sphere increases. However, this shell melts back due to the convective heat supplied by the metal bath, exposing the sphere directly to the melt with subsequent complete melting of the sphere. In this manner, the surface area of the immersed sphere increases, reaches a maximum value, and then decreases over time.

In Appendix B, a brief explanation is given based on a computational study on the melting time of 2.54 diameter spheres immersed in metal melts at different superheats. It seems that the use of the initial surface area of the sphere gives rise to not more than a 10% error in the estimation of the average surface area,

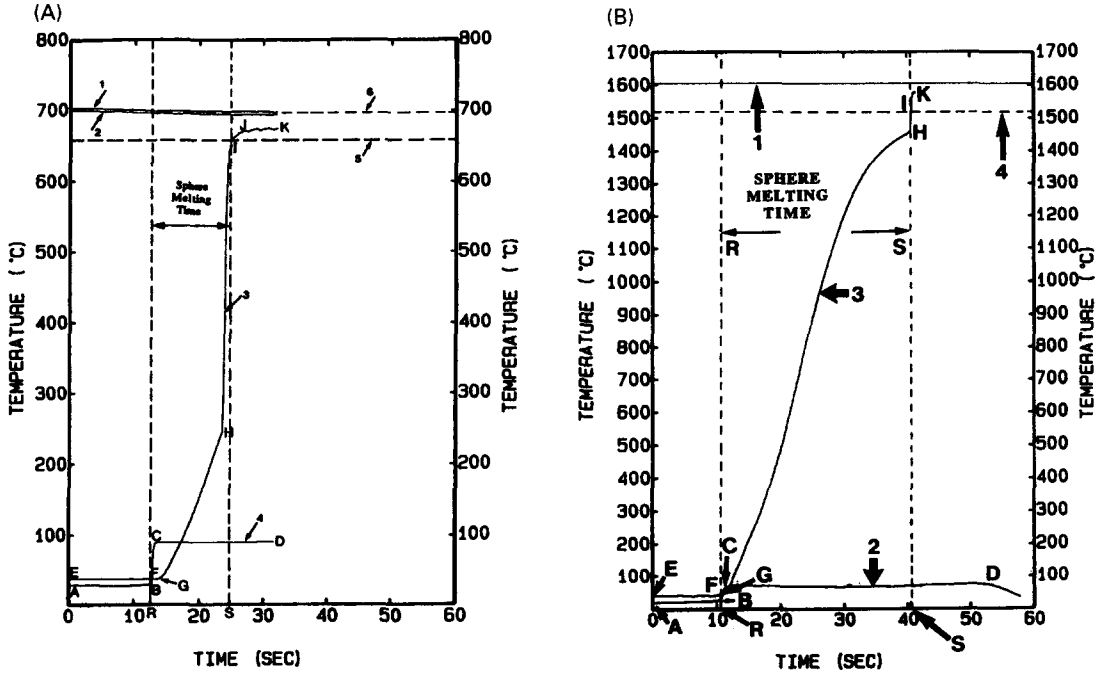

Fig. 6. (A) Typical experimental result for an aluminum natural convection experiment. Curves 1 and 2: representative bath temperature readings at different locations in the aluminum bath. Curve 3: temperature profile of aluminum sphere thermocouple. Curve 4: temperature profile of external thermocouple that records immersion time. Curve 5: aluminum melting point. Curve 6: temperature reading of independent thermocouple at the sphere immersion point at the end of the experiment. (B) Typical experimental result for a steel natural convection experiment. Curve 1: steel bath temperature. Curve 2: temperature profile of external thermocouple that records immersion time. Curve 3: temperature profile of steel sphere thermocouple. Curve 4: melting point of the steel used.

and as a result the heat flux is estimated with an error of not more than 9%. It should also be mentioned that withdrawal tests were performed on spheres under natural and forced convection conditions [26]. These tests showed that the spheres were intact for most of the immersion period. The spheres started showing signs of melting (i.e. wrinkles at their surface together with mass loss) after 85–90% of the melting time of the sphere had elapsed. From the computational as well as the experimental studies described above, it can be concluded that the initial surface area of the sphere provided a good approximation of the average surface area during an actual experiment. Equation (9) implicitly assumes that the heat losses from the sphere to the sphere holder are practically zero. In ref. [26] an analysis of heat losses through the sphere holder has found them to be very small and therefore can be ignored. The results of natural convection experiments are summarized in Table 1. All the thermophysical properties are evaluated at the film temperature. In this case, the film temperature is the average of the bath temperature and the sphere surface temperature, which is at the melting point.

RESULTS FOR PART II. FORCED CONVECTION

Figures 7(A) and (B) show typical experimental result, for spheres rotating in liquid aluminum and liquid steel, respectively. These figures illustrate how the melting time (Δt) was deduced from each experimental result. In essence, the procedure is identical to the one presented previously for the natural convection experiments. For this set of experiments, an additional parameter was recorded, which was the tangential velocity of the rotating sphere. Using similar procedures which were outlined in the results for Part I, the average convective heat flux from the metal bath was estimated (q''_D). Table 2 presents these results. As seen from Table 2 for each experimental run the ratio of Grashof vs the square of the Reynolds number is computed. This ratio was found to be always less than 0.1. For experimental runs which met this criterion, the free convection effects become negligible [27]. Experimental runs for which this criterion was not met were discarded. This occurred in cases which the liquid metal had a very large superheat and the sphere was rotating at a low tangential velocity. According to the criterion introduced by Nordlie and Kreith [27], gravitationally induced free convection could be ignored in all tests reported here so that the Nusselt, Reynolds and Prandtl numbers were the only variable parameters.

DISCUSSION

Statistical analyses of the results presented in Table 1 (i.e. natural convection) resulted in the following semi-empirical correlation:

$$\overline{Nu_D} = 2 + 10^{(-3.746)} * (Gr * Pr)^{0.878}$$

$$\text{for } 0.014 \leqslant Pr \leqslant 0.219. \quad (10)$$

The coefficient of correlation was 0.901 with a standard error of estimate 0.232 with 8 degrees of freedom. By using data from both liquid metals (aluminum and steel) to derive equation (10), its effective Prandtl range is much greater than considering either metal on its own. Therefore, equation (10) can be applied to metals with this wide range of Prandtl numbers.

In Fig. 8(A), equation (10) is presented by line 1 along with the experimental points which were used. In addition, lines 2 and 3 present predictions from theoretically derived correlations made by Raithby and Hollands [1] and Churchill [2]. These predictions were derived by applying equations (1) and (2), presented in the introduction of this paper, using the Prandtl number applicable for aluminum. As seen, the slopes of lines 2 and 3 are quite different from that of line 1. Both lines 2 and 3 overpredict the experimentally derived results for liquid aluminum. For the range of Rayleigh numbers investigated, equation (1) derived by Raithby and Hollands [1], line 2 in Fig. 8(A), over predicts the results obtained by applying equation (2) derived by Churchill [2].

Figure 8(B) displays similar findings as Fig. 8(A). In this case however, lines 2 and 3 represent predictions derived from equations (1) and (2) using the Prandtl number for steel. Lines 2 and 3 underpredict the experimentally derived results for liquid steel. Moreover, their slopes are different. In both Figs 8(A) and (B), results derived from equation (1) overpredict the results derived from equation (2). In addition, equations (1) and (2) slightly deviate from the experimental results of aluminum [Fig. 8(A)]. In the case of liquid steel the deviation is much more pronounced [Fig. 8(B)].

Statistical analysis on the results shown in Table 2 (i.e. forced convection) resulted in the following correlation:

$$\overline{Nu_D} = 2 + 1.114 * Re^{0.557} * Pr^{0.914}$$

$$\text{for } 0.014 \leqslant Pr \leqslant 0.219 \text{ and } 4330 \leqslant Re \leqslant 20780. \quad (11)$$

The coefficient of correlation was 0.991, with a standard error of estimate of 0.066 and 15 degrees of freedom. Figure 9 depicts equation (11) as it is applied to aluminum and steel (solid lines). As seen, the results for steel are higher than for aluminum. The main reason for this is the difference in Prandtl numbers, Pr for steel is 0.197, while Pr for aluminum is 0.014.

In addition, Fig. 9 presents for both metals predictions from theoretically derived equations by Hsu [17] and Sideman [18]. As seen, these predictions for the case of liquid aluminum are much higher than the experimental results. Predicted estimates based on theoretical analyses by Hsu [17] and Sideman [18] have been found to be higher than experimentally

Table 1. Experimental results and calculations in natural convection

Run no.	Liquid metal	Melting time [s]	Liquid metal temperature [°C]	Heat transfer coefficient h_D [W m^{-2}*K^{-1}]	Average heat flux q''_D [kW m^{-2}]	Nusselt, Nu_D	Grashof, Gr_D	Prandtl, Pr	Rayleigh, Ra_D
1	Aluminum	17.75	702.5	16064.2	682.7	4.40	3015666.15	0.014	42586.6
2	Aluminum	17.5	702.5	16293.7	692.4	4.46	3015666.15	0.014	42586.6
3	Aluminum	17.5	702.5	16293.7	692.4	4.46	3015666.15	0.014	42586.6
4	Aluminum	10	754	12891.9	1211.8	3.49	7267788.36	0.013	97122.1
5	Steel	29	1610	17213.1	1549.1	19.22	2751447.86	0.197	542712.0
6	Steel	30.2	1610	16529.1	1487.6	18.45	2751447.86	0.197	542712.0
7	Steel	30.4	1610	16420.3	1477.8	18.33	2751447.86	0.197	542712.0
8	Steel	39	1585	17722.3	1151.9	20.61	1920862.63	0.209	402099.8
9	Steel	44	1565	22690.0	1021.0	27.31	1293735.46	0.219	284426.1

Table 2. Experimental results and calculations in forced convection

Run no.	Liquid metal	Melting time [s]	Velocity [m s^{-1}]	Temperature [°C]	Heat transfer coefficient h_D [W m^2*K^{-1}]	Average heat flux q''_D [kW m^{-2}]	Nusselt, Nu_D	Reynolds number, Re	Grashof number, Gr_D	$Gr/(Re^2)$
1	Aluminum	13.75	0.1519	702.5	20737.4	881.3	5.68	7554.16	3246961.23	0.056
2	Aluminum	12	0.237	702.5	23761.6	1009.8	6.51	11786.28	3246961.23	0.023
3	Aluminum	12.97	0.2743	702.5	21984.6	934.3	6.02	13641.25	3246961.23	0.017
4	Aluminum	10	0.3767	702.5	28514.0	1211.8	7.81	18733.72	3246961.23	0.009
5	Aluminum	9	0.3954	702.5	31682.2	1346.4	8.68	19663.69	3246961.23	0.008
6	Aluminum	9	0.499	702.5	31682.2	1346.4	8.68	24815.84	3246961.23	0.005
7	Aluminum	6	0.219	754	21486.6	2019.7	5.83	11368.74	7825207.57	0.060
8	Aluminum	5.75	0.3507	754	22420.8	2107.5	6.08	18205.56	7825207.57	0.023
9	Aluminum	4.75	0.4837	754	27141.0	2551.2	7.36	25109.87	7825207.57	0.012
10	Steel	11.5	0.32	1610	43406.9	3906.6	48.47	10066.85	2751447.86	0.027
11	Steel	20.5	0.2	1610	24350.2	2191.5	27.19	6291.78	2751447.86	0.069
12	Steel	20.2	0.2676	1585	34216.4	2224.0	39.80	8276.79	1920862.63	0.028
13	Steel	27.52	0.1726	1585	25115.2	1632.4	29.21	5338.46	1920862.63	0.067
14	Steel	22.75	0.2946	1565	43883.9	1974.7	52.81	8987.39	1293735.46	0.016
15	Steel	25.25	0.23	1565	39539.0	1779.2	47.58	7016.63	1293735.46	0.026
16	Steel	35.25	0.1417	1565	28322.2	1274.5	34.08	4322.85	1293735.46	0.069

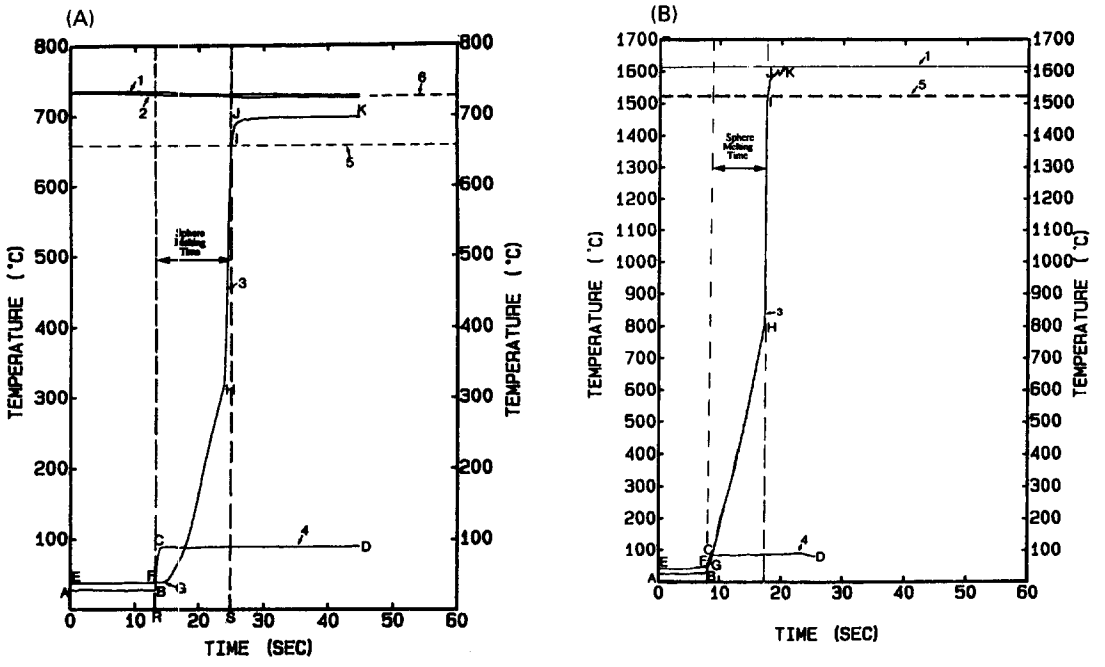

Fig. 7. (A) Typical experimental result with aluminum sphere rotating in liquid aluminum. Curves 1 and 2: representative bath temperature readings at different locations in the aluminum bath. Curve 3: temperature profile of aluminum sphere thermocouple. Curve 4: temperature profile of external thermocouple that records immersion time. Curve 5: aluminum melting point. Curve 6: temperature reading of independent thermocouple at the sphere immersion point at the end of the experiment. (B) Typical experimental result with steel sphere rotating in liquid steel. Curve 1: representative bath temperature reading. Curve 3: temperature profile of steel sphere thermocouple. Curve 4: temperature profile of external thermocouple that records immersion time.

derived results by other investigators as well, examining liquid mercury [19] and liquid sodium [20]. In the case of liquid steel, however, the theoretically and experimentally derived correlations are in relatively close agreement. In contrast to mercury, sodium and aluminum whose respective Prandtl numbers (i.e. 0.024, 0.004 and 0.014) are not very different from one another, liquid steel is distinguished by its appreciably higher Prandtl number (i.e. 0.197). It may be that the Prandtl number of liquid steel as well as the range of Reynolds number which was considered in the present experimental work with liquid steel, provided the optimal combination for a more accurate prediction from theoretically derived correlations.

Liquid metals with a low Prandtl number (i.e. mercury 0.024, aluminum 0.014, sodium 0.004), compared to those with a high Prandtl number (i.e. steel 0.197), exhibit a greater deviation between theoretically and experimentally derived data. This appears to be true for natural as well as forced convective heat transfer.

CONCLUSIONS

An experimental technique was presented to investigate natural and forced convective heat transfer in the harsh environment of liquid metals. Using this technique, the average heat flux from the metal bath to a stationary as well as to a rotating sphere can be measured. Experimental results under natural convection in liquid aluminum and liquid steel are reported. By regressing the experimental results, the following correlation was deduced:

$$\overline{Nu_D} = 2 + 10^{(-3.746)} * (Gr * Pr)^{0.878}$$

$$\text{for } 0.014 \leqslant Pr \leqslant 0.219.$$

The theoretically derived correlations of other investigators tend to overpredict the experimentally derived data for liquid aluminum. In contrast, the same correlations tend to underpredict the experimentally derived data for liquid steel.

From the experimental results under forced convection conditions, the following correlation was deduced:

$$\overline{Nu_D} = 2 + 1.114 * Re^{0.557} * Pr^{0.914}$$

$$\text{for } 0.014 \leqslant Pr \leqslant 0.219 \text{ and } 4330 \leqslant Re \leqslant 20780.$$

The theoretically derived correlations overpredict the experimentally derived results. This is especially true for metals with very low Prandtl numbers, like aluminum, mercury and sodium.

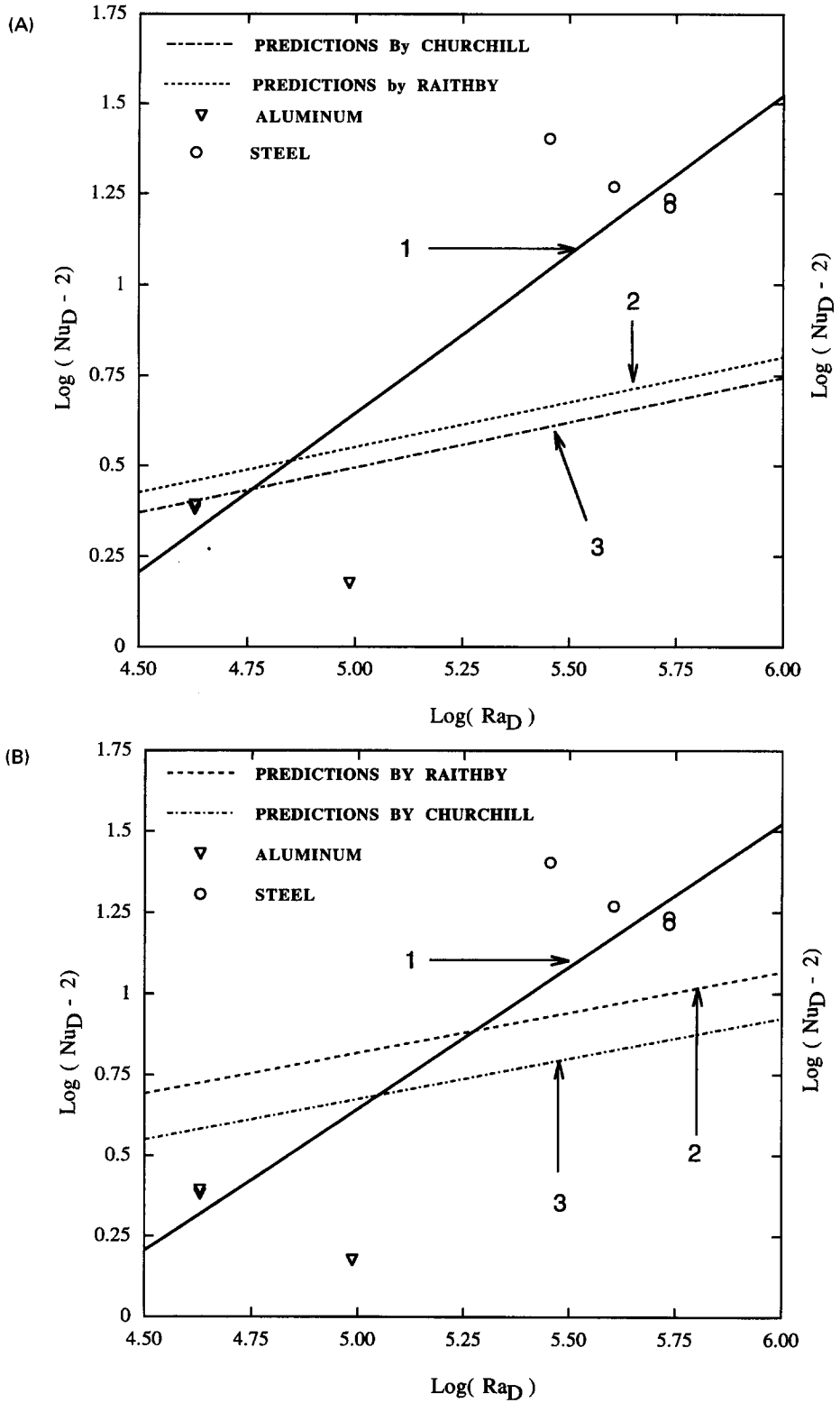

Fig. 8. (A) The average Nusselt number dependence on Ra_D for spheres. The circles represent steel experimental points and the triangles represent aluminum experimental points. Curve 1 is the graphical representation of equation (10). Curve 2 is derived from equation (1). Curve 3 represents equation (2). Both curves 2 and 3 were derived by considering liquid aluminum (i.e. Prandtl number 0.014). (B) The average Nusselt number dependence on Ra_D for spheres. The circles represent steel experimental points and the triangles represent aluminum experimental points. Curve 1 is the graphical representation of equation (10). Curve 2 derived from equation (1). Curve 3 represents equation (2). Both curves 2 and 3 were derived by considering liquid steel (i.e. Prandtl number 0.197).

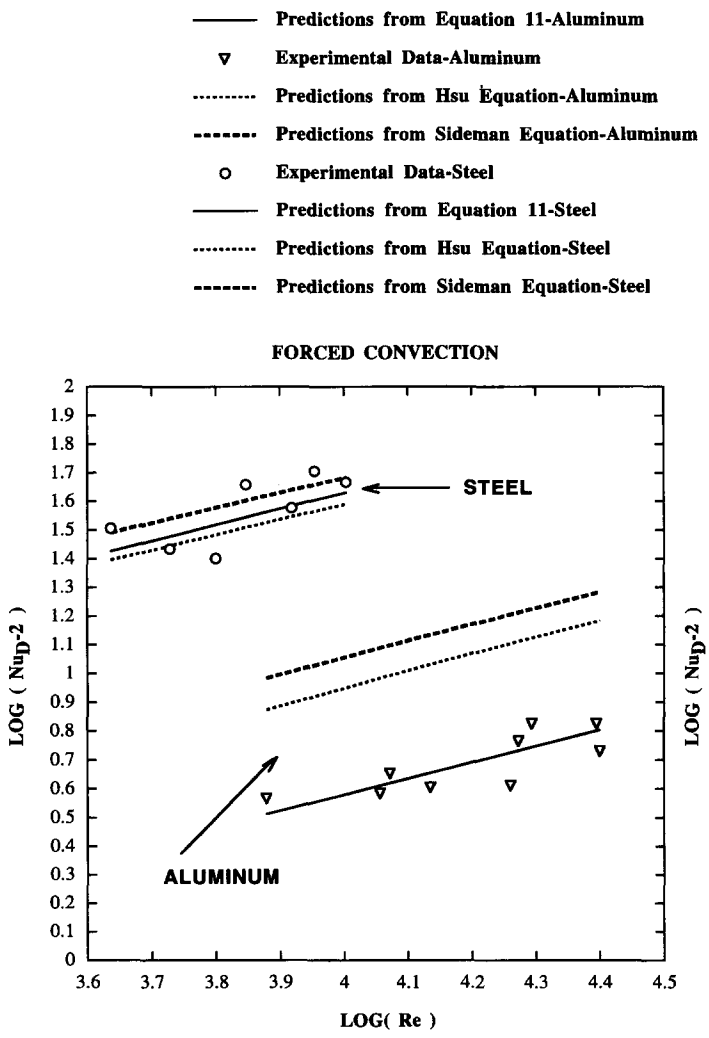

Fig. 9. Experimental results of convective heat transfer tests, average Nusselt number vs Reynolds number for aluminum and steel. In addition predictions from theoretical analysis made by Hsu and Sideman.

Acknowledgements—This work was supported by a grant from the Natural Sciences and Engineering Research Council of Canada. The authors also thank Dr P. G. Sismanis for his insight and helpful comments. In addition, the support of Electro-Nite Co. is gratefully acknowledged. Special thanks are also extended to Mr George Frigm of Electro-Nite Co. for expediting this research.

REFERENCES

1. G. D. Raithby and K. G. T. Hollands, A general method of obtaining approximate solutions to laminar and turbulent free convection problems, *Adv. Heat Transfer* **11**, 266–315 (1975).
2. S. W. Churchill, Comprehensive, theoretically based correlating equations for free convection from isothermal spheres, *Chem. Engng Commun.* **24**, 4–6 (1983).
3. R. P. Stein, Liquid metal heat transfer, *Adv. Heat Transfer* **3**, 101–174 (1966).
4. P. G. Sismanis and S. A. Argyropoulos, Convective heat transfer measurements in liquid metals under different fluid flow conditions, *Metall. Trans. B* **19B**, 859–870 (1988).
5. S. C. Heyman C. F. Bonilla and S. W. Ehrlich, Natural-convection transfer processes: heat transfer to liquid metals and nonmetals at horizontal cylinders, *Chem. Engng Symp. Ser.* **49**, 21–31 (1953).
6. T. Yuge, Experiments on heat transfer from spheres including combined natural and forced convection, *Trans. ASME, J. Heat Transfer* **82**, 214–220 (1960).
7. T. Chiang, A. Ossin and C. L. Tien, Laminar free convection from sphere, *Trans. ASME, J. Heat Transfer* **86**, 537–542 (1964).
8. G. D. Raithby, A. Pollard, K. T. G. Hollands and M. M. Yovanovich, Free convection heat transfer from spheroids, *Trans. ASME, J. Heat Transfer* **98**, 452–457 (1976).
9. W. S. Amato and Chi Tien, Free convection heat transfer from isothermal spheres to water, **15**, 327 (1972).
10. A. A. Kranse and J. Schenk, Thermal free convection from a solid sphere, *Appl. Sci. Res. A* **15**, 397 (1965).
11. F. Nils, *Geland's Beit. zur Geophys.* **52**, 170 (1938).
12. W. E. Ranz and W. R. Marshall, Evaporation from drops—I, *Chem. Engng Prog.* **48**, 141–146 (1952).
13. R. L. Steinberger and R. E. Treybal, Mass transfer from a solid soluble sphere to a flowing liquid stream, *A.I.Ch.E. Jl* **6**(2), 227–232 (1960).
14. G. Schutz, Natural convection mass-transfer measurements on spheres and horizontal cylinders by an electrochemical method, *Int. J. Heat Mass Transfer* **6**, 873–879 (1963).
15. F. A. M. Schenkels and J. Schenk, Dissolution of solid spheres by isothermal free convection, *Chem. Engng Sci.* **24**, 585 (1969).
16. S. N. Singh, Heat Transfer by laminar flow from a rotating sphere, *Appl. Sci. Res.* **A9**, 197–205 (1960).
17. Hsu Chia-Jung, Heat transfer to liquid metals flowing past spheres and elliptical-rad bundles, *Int. J. Heat Mass Transfer* **8**, 303–315 (1965).
18. S. Sideman, The equivalence of the penetration theory and potential flow theories, *Ind. Engng Chem.* **58**(2), 54–58 (1966).
19. F. Kreith, L. G. Roberts, J. A. Sullivan and S. N. Sinha, Convection heat transfer and flow phenomena of rotating spheres, *Int. J. Heat Mass Transfer* **6**, 881–895 (1963).
20. L. C. Witte, An experimental study of forced-convection heat transfer from a sphere to liquid sodium, *Trans. ASME, J. Heat Transfer* **90**, 9–12 (1968).
21. G. C. Vliet and G. Leppert, "Forced-convection heat transfer from an isothermal sphere to water, *Trans. ASME, J. Heat Transfer*, **83**(2), 163–175 (1961).
22. S. A. Argyropoulos and P. G. Sismanis, The mass transfer kinetics of niobium into liquid steel, *Metall. Trans* **22B**, 417–427 (1991).
23. J. Schade, Assimilation and recovery characteristics of cored wire ferroalloy trimming additions for ladle and tundish metallurgy, Ph. D Thesis, Department of Metallurgy and Materials Science, University of Toronto (1990).
24. AR-23 Encoder User Guide, Compumotor Division of Parker Hannifin Corporation, Rohnert Park, CA, U.S.A.
25. A. C. Mikrovas and S. A. Argyropoulos, Novel technique to estimate velocity in liquid steel and in other high temperature liquid metals, *Iron and Steelmaker*, pp. 85–93 (1993).
26. A. C. Mikrovas, Measurement of magnitude of velocity in high temperature liquid metals, Ph.D Thesis, Department of Metallurgy and Materials Science, University of Toronto (1992).
27. R. Nordlie and F. Kreith, Convection heat transfer from a rotating sphere, international developments in heat transfer, *Am. Soc. Mech. Engrs*, pp. 149–156 (1957).
28. Y. S. Touloukian, R. W. Powell, C. Y. Ho and P. G. Klemens, Thermophysical properties of matter, *The TPRC Data Series*, Vol. 1, p. 9. IFI/Plenum Press, New York (1970).
29. Aluminum properties and physical metallurgy, American Society for Metals (1984).
30. *Smithels Metal Reference Book* (6th Edn) (Edited by E. A. Brandes). Butterworths, London (1983).
31. E. T. Turkdogan, *Physical Chemistry of High Temperature Technology*. Academic Press, New York (1980).

APPENDIX A

The data collected on the thermodynamic, thermal, and physical properties of aluminum and steel, which were used in this study, are those reported in refs. [28–31]. To calculate the total heat required for melting (ΔH) the following values were used: for aluminum (ΔH) = 1059 kJ kg^{-1}, for steel (ΔH) = 1360 kJ kg^{-1}. Table A1 presents some data related to liquid aluminum and liquid steel.

Table A1. Thermophysical properties used

Property	Aluminum	Steel
Thermal conductivity [W mK^{-1}]	95.4	35
Heat capacity [J kg^{-1} K^{-1}]	1080	795
Density [kg m^{-3}]	2374 [973 K]	6941 [1893 K]
Viscosity [kg s^{-1} m^{-1}]	1.15×10^{-3} [973 K]	5.13×10^{-3} [1893 K]
Coefficient of thermal expansion [K^{-1}]	1.17×10^{-4}	1.26×10^{-4}

APPENDIX B

A mathematical model was developed which numerically solves the heat conduction equation in spherical coordinates. This model simulates the shell formation when a solid sphere at room temperature is immersed in liquid metal. In addition, this model predicts the time required for the sphere to melt. This model was used to simulate the melting behavior of a 2.54 cm diameter solid sphere immersed in identical metal baths. In making these predictions, experimentally measured convective heat transfer rates were used [4]. In Tables B1 and B2 some results of this computational work are presented. In both tables the average radius column indicates the average radius of the sphere during its entire melting period. The melting time column corresponds to the total melting time of the sphere. The error in average sphere radius is calculated from the following formula:

$$\text{Error} = ((\text{RAD} - \text{AVERAD})/\text{Rad}) \times 100 \qquad \text{(B1)}$$

where RAD, represents the initial sphere radius (i.e. 0.0127 m); AVERAD, computed average sphere radius and Error: estimated error involved [%].

From Tables B1 and B2, for the liquid metal superheats examined, it is clear that the error involved, considering the initial sphere radius instead of the average sphere radius, is less than 10%. Thus, it was considered reasonable to base the calculations for the heat fluxes on the initial surface area of the sphere, since the underestimation of the lateral surface area in the shell period is compensated by its overestimation in the subsequent melting period of the sphere.

Table B1. Computational work with a steel sphere

Steel bath superheat [K]	Average radius [m]	Melting time [s]	Sphere radius average error [%]
50.0	0.01299	66.70	−2.35
60.0	0.01269	51.80	−0.03
70.0	0.01236	41.81	2.66
100.0	0.01183	26.88	6.84

Table B2. Computational work with aluminum sphere

Aluminum bath superheat [K]	Average radius [m]	Melting time [s]	Sphere radius average error [%]
40.0	0.01247	30.17	1.75
50.0	0.01228	25.84	3.28
60.0	0.01172	21.62	7.70
70.0	0.01166	19.34	8.16